Chemo-mechanical behaviour of non-expansive clays accounting for salinity effects

Géotechnique

Chemo-mechanical behaviour of non-expansive clays accounting for salinity effects

GEOT-2021-183 | Paper

Submitted by: Guido Musso, Giulia Scelsi, Gabriele Della Vecchia

Keywords: CLAY MINERALOGY, CONSTITUTIVE MODELLING, FABRIC/STRUCTURE OF SOILS, SUCTION, YIELD LOCUS

Chemo-mechanical behaviour of non-expansive clays accounting for salinity effects

Guido Musso[1], Giulia Scelsi[2] and Gabriele Della Vecchia [3]

1. Professor
Department of Structural, Geotechnical and Building Engineering
Politecnico di Torino
Corso Duca degli Abruzzi, 24
10129 Torino, Italy
guido.musso@polito.it

2. Ph.D
Department of Civil and Environmental Engineering,
Politecnico di Milano
Piazza Leonardo da Vinci, 32
20133 Milano, Italy
giulia.scelsi@polimi.it

3. Associate Professor
Department of Civil and Environmental Engineering,
Politecnico di Milano
Piazza Leonardo da Vinci, 32
20133 Milano, Italy
gabriele.dellavecchia@polimi.it

Abstract

Changes in the chemistry of the pore fluid are known to impact on the hydro-mechanical behaviour of clays. Experimental evidence collected in the last decades led to the formulation of constitutive chemo-mechanical models for expansive soils used in engineering practice for the containment of pollution, such as bentonite. Less attention has been paid to modelling the chemo-mechanical behaviour of non-expansive clays, less frequently used for geoenvironmental applications but equally exposed to chemical changes.

First key differences between the impact of salinity on the fabric of expansive and non-expansive clays are pointed out. At the macroscopic scale, an increase in salinity causes a small translation of the Normal Compression Line of non-expansive clays to higher void ratios, which in some cases is also accompanied by an increase in compressibility. The opposite occurs for expansive clays. These experimental evidences provide the basis for a chemo-mechanical model formulated in the frame of elasto-plasticity with generalised hardening, whose yield surface expands with pore fluid concentration. The model is validated against experimental results, both original and from the literature. Simulation results compare very well with those of tests performed on reconstituted, compacted and intact samples.

1 - Introduction

Pore fluid chemistry is well known to influence the hydraulic and mechanical behaviour of clays (see e.g. the comprehensive summary in Sridharan, 1991). This influence is due to the effects that the pore fluid composition has on superficial forces, such as van der Waals and electrostatic interactions, which act between close particles (see e.g. van Olphen, 1977, Santamarina et al., 2001). van der Waals interaction is always attractive and mainly depends on the dielectric constant of the pore fluid, while it is practically independent on the type and concentration of dissolved ions.

Electrostatic forces are caused by the electrical charge of the particle surface, and are mediated by the Diffuse Double Layer (DDL) of ions of opposite charge with respect to the one of the particle surface. As the solute concentration increases, the thickness of the DDL decreases and so do electrostatic forces. Particles of most clay minerals have a platy thin shape with large faces and thin edges. The electrical charge on the particles face is mainly caused by the isomorphous substitution in the crystal lattice of higher valence metals with lower valence metals (e.g. Mitchell and Soga, 2005): it is negative and not very influenced by pore water composition. The electrical charge on the particle edge is caused by the interruption of the crystal lattice, which exposes metals and hydroxyl groups to the surface: it is usually positive (van Olphen, 1977), and it can be influenced by the composition of the pore water because of the adsorption/desorption of protons and other ions (Santamarina et al., 2001). This is particularly relevant for kaolinite: as the pH grows the positive edge charge decreases and becomes negative at high pHs (e.g. Sposito 1984).

The interplay between van der Waals attractive forces and electrostatic forces (which are repulsive between particles faces, attractive between edges and faces) determines the type of association of the particles in suspensions and the fabric imparted through sedimentation. According to Santamarina et al. (2002), the ratio between the length and the thickness of the particles determines the relevance of the different forces. Particles of expansive clays, such as montmorillonite, are extremely elongated and thin. Edge charges have then very little relevance on their interaction and in suspensions they tend dispose according to a face to face association (i.e. they *aggregate*). This association dominates their fabric and as at high ionic concentrations more cations are available to shield the face negative charge the thickness of the double layer and the size of the pores in the aggregates reduces.

Particles of non-expansive clays, such as illite and kaolinite, have a smaller length to thickness ratio (i.e. they are relatively thicker) and attraction between particles edges and faces, or even between edges, can be relevant when they are in suspensions. The term flocculation is used to describe single particles, or groups of aggregated particles, associated according to a face to edge or edge to edge scheme. The association of kaolinite particles is ruled both by pH and ionic concentration (Palomino & Santamarina, 2005). Aggregation takes place above a threshold ionic concentration (NaCl molarity of the order of 10^{-1} M): edge to face flocculation of aggregates occurs at both very low and very high pHs, while it has not been observed for pHs ranging between 5 and 7. Below the threshold ionic concentration aggregation occurs without flocculation when the pH is smaller than 3, while edge to face flocculation occurs at higher pHs. Not much attention has been paid to the role of pH for illite. As for the role of pore fluid salinity, the experience gathered for Norwegian illitic quick clays suggests that sedimentation in brackish

or marine water promotes edge to edge flocculation (i.e. a cardhouse type of fabric), which collapses after exposure to fresh water (see e.g. Rosenqvist, 1966). The same evidence has been reported for non-expansive smectites from Japan (Ariake clay, Ohtsubo et al.,1985).

The fabric of a given clay soil depends on the relative magnitude of superficial, body and mechanical forces when it is formed. While surface forces dominate on body and mechanical forces for suspensions and slurries, the opposite holds for compacted soils. The relevance of the soil formation stage, and in general of fabric, on the soil hydro-mechanical response has been clearly highlighted by Collins and Mc Gown (1974) according to which, although the fabric of soils "*cannot be expected to be determined simply on basis of the depositional history and environment, it has been found that there may be a dominant feature or set of feature present in any one soil. This predominant microfabric can induce certain types of engineering behaviors, such as sensitivity, collapse and expansion*".

The impact of fabric on different aspects of the clay behaviour, and particularly on those related to the pore fluid chemistry imposed during preparation of reconstituted or compacted specimens, has been documented in many experimental works. The one-dimensional compression curves of samples reconsolidated from slurry have been found to depend on the pore fluid of preparation for kaolinite and bentonite saturated with fluids with different dielectric constant (Sridharan & Rao, 1973) and smectitic soils saturated with brines (Barbour & Yang, 1993, Di Maio, 1996). Barbour & Yang (1993) further remark that adding brine to montmorillonite material prior to static compaction in unsaturated conditions causes the moisture-density relationship to be altered due to physicochemical effects, which leads to compression curves which depend both on the preparation procedure and on the pore fluid chemistry.

Modifications of pore fluid chemistry are also possible due to pore fluid replacement or of diffusion of the solutes, and pore water chemistry is expected to change with time in many earth structures devoted to pollution containment. For example, in compacted clay barriers for nuclear waste storage, chemical changes can occur due to the inflow of water from the host rock and because of the evaporation triggered by temperature increase induced by radioactive reactions. In both cases, a variation of the concentration of the species dissolved in water is anticipated. In clay barriers for municipal waste disposal, the pore fluid chemical composition changes with the transport of domestic leachate, while cutoff walls encapsulating polluted sites can be progressively permeated by the contaminants spilled underground. Pore fluid chemistry also varies in natural environments, e.g. in clay formations that were deposited in marine environments that emerged in relatively recent geological times. After emersion, salt diffusion towards the boundaries of the formation or entrance of fresh water (i.e. leaching) are anticipated.

As changes in the pore fluid chemistry modify the interaction between particles, deformations even at constant total stress and impact on the hydro-mechanical properties are expected. Volume change caused by pore fluid replacement under a constant vertical stress and their effects on the following compression behaviour were studied among others by Sridharan & Rao (1973), Torrance (1974), Di Maio (1996), Musso et al., (2003, 2013). Torrance (1974) leached with distilled water undisturbed samples of Norwegian quick clays, originally filled with marine water: this process induced shrinkage in normally consolidated samples and swelling of highly over-consolidated samples.

To account for these effects, elastic-plastic chemo-hydro-mechanical models (e.g. Hueckel, 1997; Loret et al., 2002; Gajo & Loret, 2003; Liu et al., 2005; Guimaraes et al., 2013, Witteveen et al., 2013, Della Vecchia & Musso, 2016, Yan, 2018, Della Vecchia et al, 2019) were formulated in the paste decades Limited efforts have been devoted to modeling the behaviour of non-expansive clays, since excluding Witteveen et al.(2013) all of these works make specific reference to very expansive clays (bentonites, mostly relying on the experimental data from the seminal paper of Di Maio, 1996).

This work aims at formulating a simple phenomenological elasto-plastic model for the chemo-mechanical behaviour of non-expansive illitic and smectitic clays. First, the different effects of salinity on the behaviour of expansive and non-expansive clays are explored. The paper focuses then on non-expansive clays, exploring the relationship between pore fluid salinity, clay fabric and void space. The experimental behaviour of oedometer reconstituted samples of a smectitic non-expansive clay under the effects of mechanical loads imparted at different constant pore fluid compositions and of salinity changes imparted at constant vertical stress is discussed. The experimental results are exploited to formulate a constitutive model in the framework of elasto-plasticity with generalized hardening. The model was then used to simulate the results of experimental tests, both original and from the literature, performed on samples of different soils and with different initial fabrics (reconstituted from slurry, undisturbed and statically compacted samples). In all these cases, a very good agreement between model predictions and experimental data was found.

2. Influence of pore fluid salinity on the liquid limit of active and inactive clays

As recalled by Jang and Santamarina (2016), liquid limit determinations account for the mass of water which is both adsorbed onto the particle surfaces and held within the fabric. Comparing the liquid limits obtained using different saline solutions reveals then the impact of the pore fluid composition on the fabric of a given clay in slurry state. However, expressing the results of the liquid limit tests in terms of the ratio between the mass lost through heating in the oven to the non-evaporated mass is here inappropriate, since dissolved salts don't evaporate and they would be improperly considered as solid fraction. Furthermore, as the density of a solution depends on the solute concentration and the fabric is related to the type and volume of voids in the soil, the comparison between liquid limits at different salinities is more significant if expressed in terms of void ratio e_L instead of gravimetric water content w_L.

The effects of water salinity on the liquid limit was analysed for the soils listed in Table 1, where mineralogical compositions are also provided. The corrections required to the measurements of the mass lost in the oven were carried out accordingly to the procedure described in Noorany, 1983. The data set includes pure clays (kaolinite, illite and bentonite), as well as natural soils from Italy, Norway and Japan. Both data from the literature and original determinations are considered. The original determinations include a pure illite from Hungary (provided by BAAN industrial materials, Formigine, Italy), a commercial sodium bentonite which was mixed with the illite (provided by Laviosa Chimica Mineraria, Livorno, Italy), and Spigno Monferrato clay, a natural clay proceeding from the Langhe region of Italy which has been the seat of diffuse slope

instabilities promoted by the dilution of the interstitial pore water (Musso et al., 2008; Musso et al., 2017). Spigno Monferrato is a mixture of nontronite (a non-expansive ferrous smectite), illite and chlorite.

Table 1 also reports the void ratio at liquid limit obtained mixing the powder of these clays with distilled water, e_L^0, which ranges from 0.80 (Asrum clay) to 10.80 (Ponza Bentonite). The normalised ratio e_L/e_L^0 is then used in Figure 1 to show in a single graph the effects of salinity on the liquid limits of the different soils. Three different trends can be observed: e_L decreases with salinity in the case of pure expansive minerals (Ponza Bentonite) and of clays containing expansive minerals (75 illite 25 bentonite, Marino clay); it remains about constant or increases very mildly with salinity for Spigno Monferrato clay, illite and kaolinite; it increases sharply in the case of quick clays from Norway (Asrum and Drammen clay) and Japan (Ariake clay).

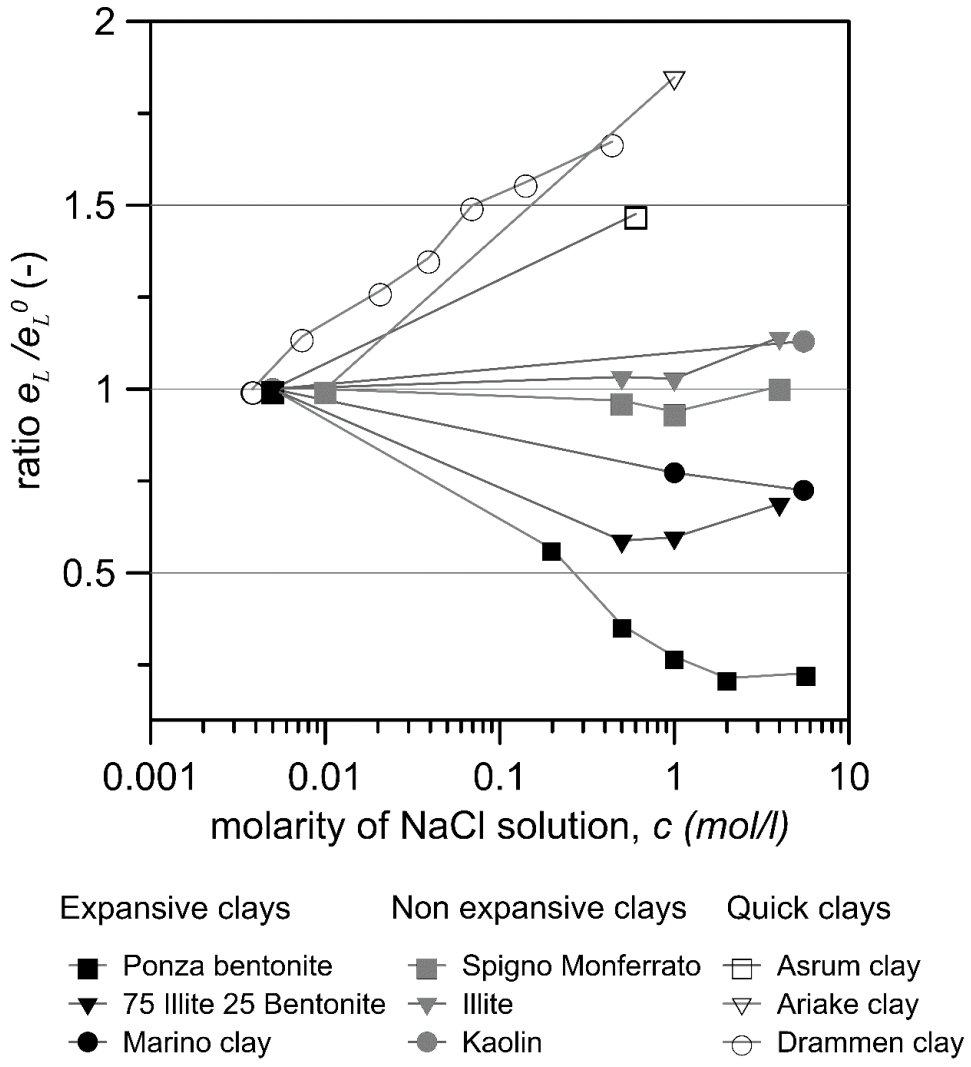

Figure 1 – Dependency of the void ratio at liquid limit e_L on NaCl molarity of the pore fluid for different clays

194 Table 1 – Mineralogy and index properties with distilled water as saturating fluid for different clay

195 soils

Soil	Reference	Main minerals	Liquid limit w_L (%)	Void ratio at liquid limit with distilled water e_L^0 (-)
Ponza Bentonite	Di Maio (1996)	montmorillonite 80% kaolinite 20%	390	10.80
75 Illite – 25 Bentonite	This study	illite 75 % bentonite 25 %	161	4.43
Ariake clay	Ohtsubo et al. (1985)	beidellite type, non-expansive smectite 46% Illite	89	2.54
Ilite	This study	illite > 95 %	83	2.26
Kaolin	Di Maio et al (2004)	kaolinite 75-80% illite 8-10%	50	1.37
Marino clay	Di Maio et al. (2004)	kaolinite 30% illite 10 % mixed illite – expansive smectite 10%	50	1.52
Spigno Monferrato	This study	nontronite, non expansive smectite illite,	41	1.13

		chlorite		
Drammen clay	Torrance (1974)	Illite Chlorite	32	0.88
Asrum clay	Bjerrum and Rosenqvist (1956)	Illitic clay	29	0.79

196

197 The results for the expansive soils agree with the observations of Sridharan et al. (1986),
198 according to whom their liquid limit is mostly ruled by effect of the reduction with salinity of the
199 thickness of the double layer on the particles face. This appears not to be the case with the other
200 materials. The increase of e_L with salinity for the quick clays is consistent with the flocculated
201 fabric exhibited by these soils in saline water, which is lost upon exposure to fresh water
202 (Rosenqvist, 1966, Torrance & Ohtsubo, 1995). The flocculated fabric implies larger pores than
203 the aggregated fabric, explaining the increase of e_L with salinity. A similar phenomenon is
204 expected for the pure illite. While the liquid limit of kaolinite is controlled mostly by the pH while
205 it is not much affected by salinity alone (Sridharan et al., 1988), the kaolin considered in Figure 1,
206 proceeding from the work of Di Maio et al. (2004) contains a 10 % fraction of illite, which might
207 justify the increase of e_L with salinity, while the different behaviour of different minerals might
208 explain the trend of e_L for Spigno Monferrato clay, where e_L decreases slightly at lower salinities
209 and increases at higher salinities.

210

211

3. Compression behaviour of non expansive clays along chemo-mechanical paths

3.1 Elastic and elasto-plastic compliance along constant salinity paths

As salinity can impact on the fabric and liquid limit of clays, it is expected to affect also their behaviour along compression. The dependency of oedometer compressibility on the salinity (NaCl concentration) of the pore water for the soils listed in Table 1 and a few other materials from the literature is shown in Figure 2. All the samples considered were loaded while saturated with the water of preparation (i.e. no replacement of the pore fluid have been performed). Compressibility is here expressed in terms of elastoplastic and elastic logarithmic compliance, λ and κ respectively:

$$\lambda = -\frac{\Delta e}{\Delta ln\sigma'} \quad (1)$$

$$\kappa = -\frac{\Delta e}{\Delta ln\sigma'} \quad (2)$$

λ was evaluated along the virgin loading branch in the stress range between 150 kPa and 300 kPa, while κ was determined along the unloading branch. The relationship between λ and salinity is similar to the one between e_L and salinity: λ decreases dramatically with concentration for soils containing expansive minerals, it has a moderate increment with concentration for the illite and for the quick clays, and it remains about constant for kaolin and Spigno Monferrato clay. The influence of salinity on κ is generally very small. While most data refer to reconstituted conditions, Figure 2 also reports data of an intact sample of Drammen clay (Torrance, 1974) and

235 of a compacted low-activity illitic clay (Witteveen et al., 2013). The compliance of the intact
236 Drammen clay is higher than the one of the reconstituted Drammen clay, but the role of pore
237 fluid chemistry is similar, as λ moderately increases with the concentration in both cases. No
238 measurable effects of the pore fluid concentration on compliance were found for the illitic clay
239 in Witteveen et al. (2013). Ù
240
241
242

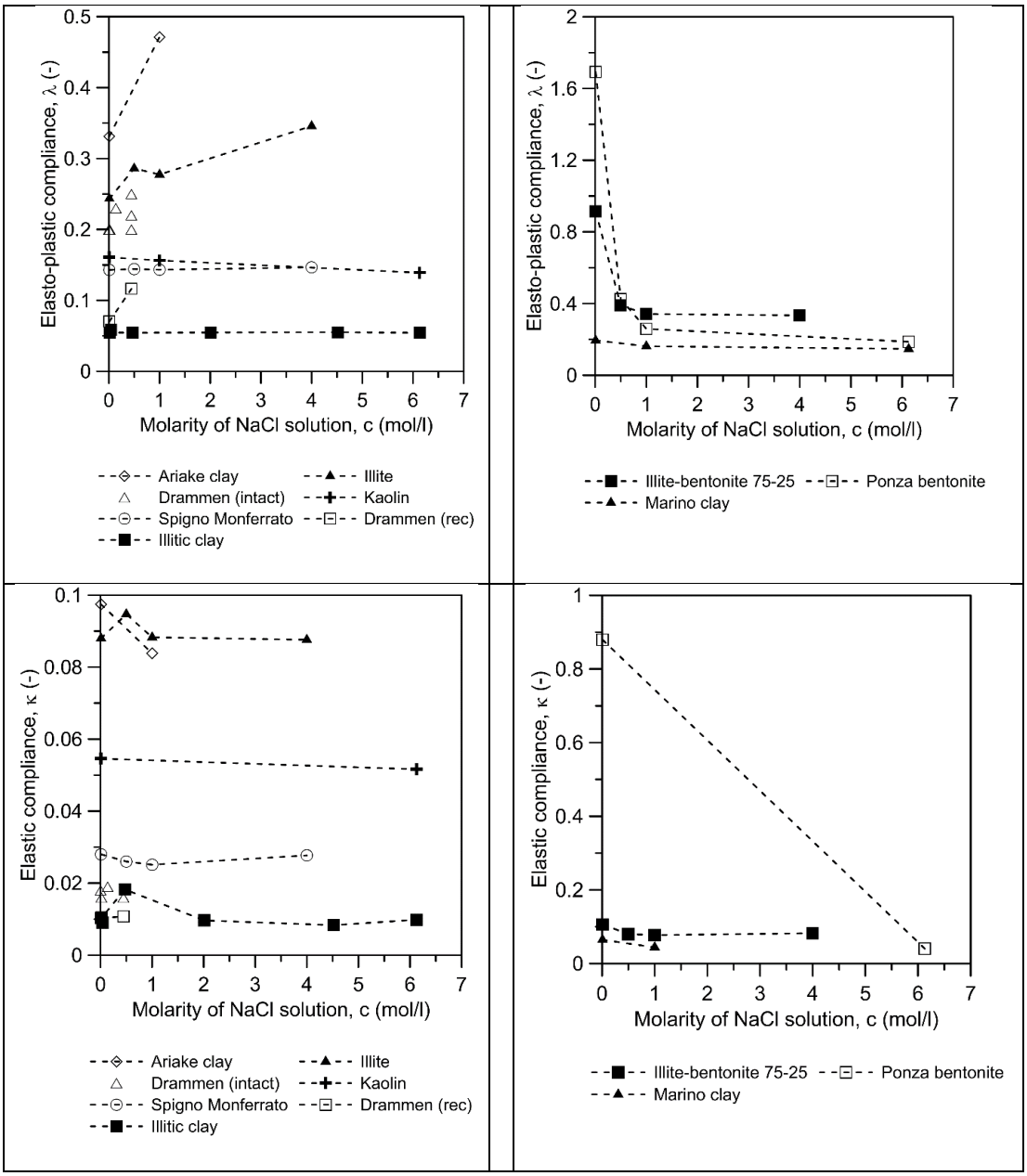

243

244 Figure 2 – Dependency of soil compressibility on NaCl molarity for different clays. (a) elasto-
245 plastic compliance of non-expansive clays, (b) elasto-plastic compliance of expansive clays, (c)
246 elastic compliance of non-expansive clays, (d) elastic compliance of expansive clays

3.2 Compression curves of non-active clays and relationship with fabric

The salinity of the pore water of preparation might affect the compression behaviour also by impacting on the position of the Normal Compression Line (NCL), i.e. on the void ratio associated to first loading under a given effective stress. Restricting the analysis to the soils tested in the present work, Figure 3 provides the experimental results for the illite and Spigno Monferrato samples. All the specimens were reconstituted and they were prepared by mixing the dry soil powder with the mass fluid required to impose an initial void ratio $e \cong 1.2\, e_L$. Distilled water and NaCl solutions with different molarities (0.5 M, 1 M, 4M) were used. For both soils, salinity has a small effect on λ, but its increase translates the NCL to higher void ratios. The opposite effect occurs for expansive soils, whose NCL moves to lower void ratios as salinity increases (see e.g. Di Maio, 1996).

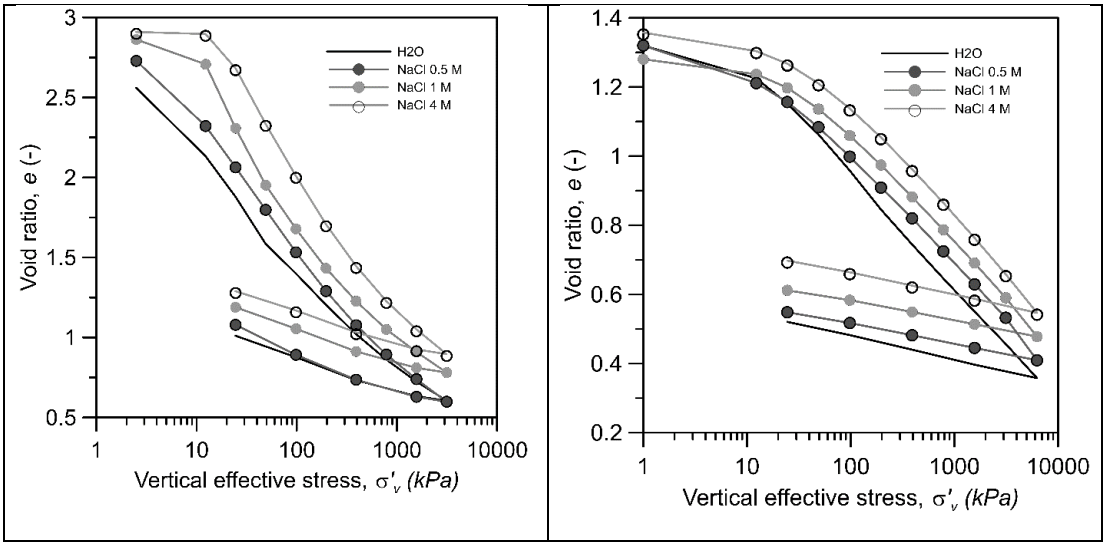

Figure 3 – Oedometer compression curves of illite (left) and Spigno Monferrato clay (right) saturated with NaCl solutions of different molarity

The effects of salinity on the compression behaviour descend from the effects of salinity on fabric. Different microstructural analyses were conducted on specimens normally consolidated at a vertical stress σ'_v = 98 kPa. All specimens were freeze dried before microscopic analysis, to avoid modifications of the pore network due to water evaporation in natural conditions.

Scanning Electron Microscope (SEM) images of the illite specimens prepared with distilled water and with the 4 M NaCl solution are presented in Figure 4. The differences between the two fabrics is very clear. The distilled water specimen (Fig. 4a and 4b) has a void ratio *e* = 1.45 and its particles are mostly aggregated parallel one to the other in a face to face arrangement, with elongated pores whose main apertures have size of the order of about 1 μm. The 4 M NaCl specimen (Fig. 4c and 4d) has a larger void ratio *e* = 1.98. A cardhouse fabric emerges, with particles disposed in an edge to edge arrangement, forming larger pores with diameters of the order of 5 – 10 μm. Notwithstanding the load that was applied, the flocculated fabric imparted to the specimen mixing the soil with highly saline water is still evident, which explains the higher void ratio of this specimen with respect to those prepared at lower salinities.

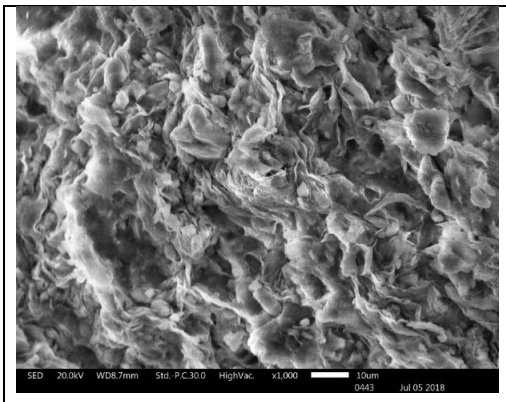

a) e = 1.45

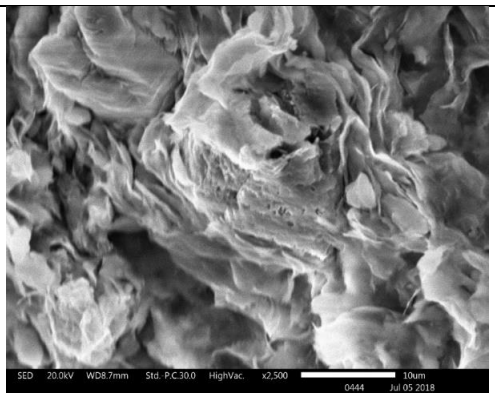

b) e = 1.45

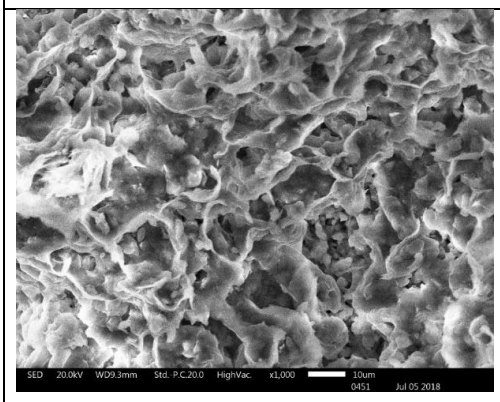

c) e = 1.98

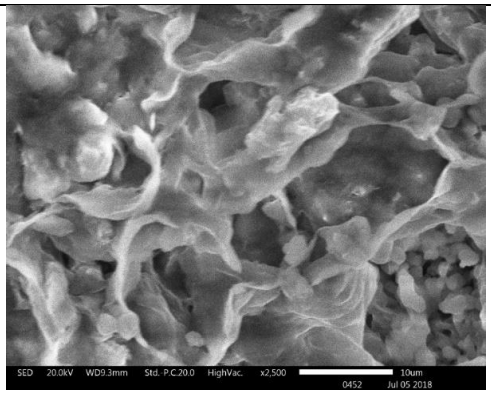

d) e = 1.98

Fig. 4 SEM images of reconstituted illite specimens prepared at e = 1.2 e_L and loaded to 98 kPa. Pore fluid is: (i) distilled water for images a) and b); (ii) 4 M NaCl solution for images c) and d). Bar length is 10 μm in all pictures

The effects of salinity on the fabric of Spigno Monferrato clay were investigated by means of Mercury Intrusion Porosimetry (MIP) tests, performed on the specimens prepared with distilled water and with the 4 M NaCl solution. The Pore Size Density function (PSD) curves of these specimens are presented in Figure 5: they show a peak in correspondence of a pore radius slightly smaller than 1 μm and they almost overlap at smaller radii. However, the saline specimen has a

287 significant fraction of larger pores with radii ranging from 1 to 10 μm, which is not present in the
288 distilled water specimen. This is consistent with the interpretation provided for the fabric of
289 Spigno Monferrati clay, that is characterized by larger voids in the presence of saline pore fluid.
290

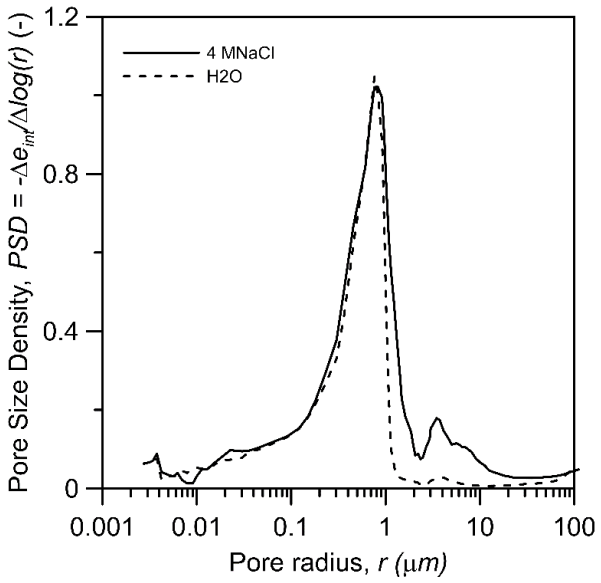

291

292 Fig. 5 PSD curves of reconstituted Spigno Monferrato specimens prepared at their liquid limit
293 and loaded to 98 kPa.
294

295

296 ## 3.3 Chemo mechanical loading paths: evidences on reconstituted Spigno
297 Monferrato clay
298

299 To investigate the combined effects of mechanical and chemical solicitations, a chemo-
300 mechanical loading path was imposed on a reconstituted specimen of Spigno Monferrato clay,
301 according to the sequence shown in Figure 6, while the experimental results in the compression
302 plane are provided in Figure 7. A slurry specimen was prepared using distilled water to obtain an
303 initial void ratio $e_0 = 1.2\ e_L$ and then placed in an oedometer.

304 Distilled water was poured in the oedometer cell and mechanical loading was applied by doubling
305 the vertical stress every 24 hours up to σ'_v = 196 kPa (point A in Figures 6 and 7). This vertical
306 stress was kept for 24 hours and then the fluid in the cell was replaced with a 4 M NaCl solution,
307 renewed daily to ensure constant salt concentration of the pore fluid at the boundary of the
308 specimen. The slow process of cation diffusion from the oedometer cell to the interior of the
309 specimen caused volume change to occur along time (i.e. osmotic consolidation, according to
310 Barbour & Fredlund, 1989). The corresponding volumetric strain took place in about 1 week. As
311 it can be appreciated in Figure 7, a decrease in void ratio occurred (Point A' in Figures 6 and 7).
312 To remove the effects that imparted by creep (as suggested by Torrance, 1974), in Figure 7 the
313 void ratios under the mechanical loads refer to the end of mechanical consolidation, while the
314 changes in void ratio measured during the chemical loads were corrected removing the effects
315 of secondary compression, expected to grow linearly with the logarithm of time.
316 A mechanical loading sequence started again with the saline solution as pore and cell fluid. Small
317 stress increments were initially applied to appreciate possible effects of the chemical history on
318 the mechanical behaviour, i.e. to detect as precisely as possible any change in preconsolidation
319 pressure. Under a vertical effective stress σ'_v = 780 kPa (point B), the procedure was inverted and
320 the cell fluid was replaced with distilled water, renewed daily to ensure constant fluid
321 composition at the specimen boundary. As long as the NaCl ions diffused outside of the specimen,
322 the specimen progressively shrank and the void ratio reduced (point B' in Figures 6 and 7). Load
323 increments were then imposed at constant pore fluid composition, again paying attention to the
324 identification of preconsolidation pressure evolution. Another salinisation step was performed
325 under a vertical effective stress σ'_v = 1600 kPa with a small decrease in the void ratio from

e = 0.59 to e = 0.58 (points C and C'). The following loading and unloading were performed at constant salinity.

As evident from Figure 7, the stress increments which immediately followed the first salinisation were characterised by an increase in stiffness (i.e. smaller compliance) with respect to the previous ones, so the experimental points do not align with the projection of the compression line deduced for the previous steps with distilled water as saturating fluid. A larger compliance was recorded again for the stress increment between 600 and 780 kPa. Salinisation appears thus to provide a sort of preconsolidation, causing an apparent OCR of the order of 2.5 – 3. A small preconsolidation effect also occurred with the salinization step imposed at σ'_v = 1600 kPa. On the other hand, after desalinisation (e.g. between points B' and C) the compliance that was registered immediately is comparable to one of the virgin material, and no preconsolidation effects were observed.

It is interesting to observe that, on the compression plane, the points which correspond to saturation with distilled water align reasonably well along a certain Normal Compression Line. The 'normally consolidated' points (i.e. for which the apparent OCR is 1) of the 4 M NaCl condition align instead along another NCL. The position of the NCL of the specimen that was prepared and loaded with the 4 M NaCl solution is also drawn in Figure 7. It can be appreciated that the NCL for the condition of preparation with distilled water and loading with 4 M NaCl lays between the NCL of preparation and loading with distilled water and the NCL of preparation and loading with brine.

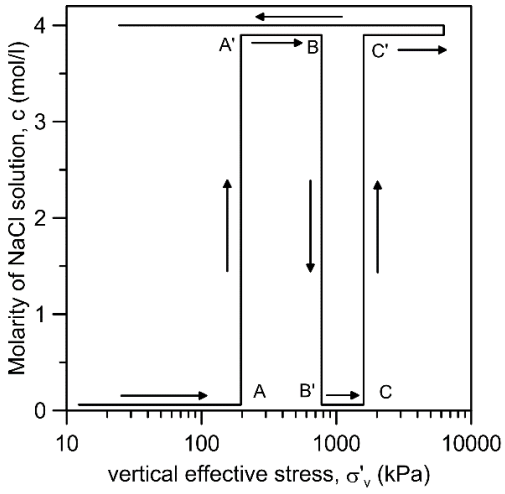

Fig. 6 Chemo-mechanical loading path imposed to reconstituted Spigno Monferrato clay

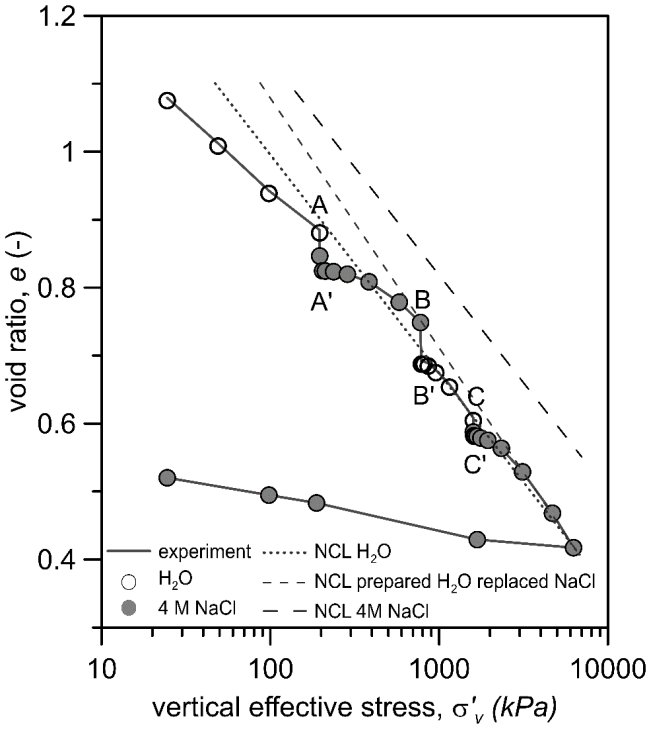

Fig. 7 Compression curves of reconstituted Spigno Monferrato clay, subjected to chemo-mechanical loading path

4 An elasto-plastic model for the chemo-mechanical behaviour of non-expansive clays

The experimental evidences collected in the previous sections provide the basis for the formulation of a simple phenomenological constitutive model capable of predicting the mechanical response of non - expansive clays subject to salinity changes. The model is developed in the framework of elasto-plasticity with generalized hardening (see, e.g., Della Vecchia et al, 2013, Tamagnini & Ciantia, 2016). The role of pore fluid chemistry on the mechanical response is assumed to directly influence both the constitutive stress and the evolution of the internal state variable.

4.1 Stress variables

The model is based on the definition of a mechanical constitutive stress variable, to reproduce mechanical solicitations, and one environmental process variable to account for changes in the chemistry of the pore fluid. The mechanical variable is the Terzaghi effective stress tensor, with components σ'_{ij}:

$$\sigma'_{ij} = \sigma_{ij} - u\delta_{ij} \quad (3)$$

where σ_{ij} is the total stress, *u* is the pore fluid pressure and δ_{ij} is the Kronecker's delta. The role of cation exchange is here neglected and the osmotic suction π is adopted as chemical process variable. The general expression for π is :

$$\pi = -\frac{RT}{v_w} ln(a_w) \quad (4)$$

where R is the universal gas constant (8.31 J mol^{-1} K^{-1}), T is the absolute temperature, v_w is molar volume of water and a_w is the activity of water, which depends on the concentration of dissolved salts. At low concentrations the van't Hoff equation can be used:

$$\pi = icRT \quad (5)$$

where i is the number of species in which the salt dissolves (e.g. 2 for NaCl and 3 for $CaCl_2$) and c is the molar concentration of the electrolyte. For molar concentrations below 1 mole/liter, the error introduced by van't Hoff equation is smaller than 5 % (Mitchell & Soga, 2005).

For the sake of simplicity, the usual volumetric and deviatoric decomposition of the stress and strain tensor in axis-symmetric conditions is introduced in the following.

4.2 Elastic behaviour

Elastic volumetric strain increments are split into two contributions, one due to mechanical loading, $\dot{\varepsilon}^e_{v\,mec}$ and the other due to osmotic suction changes, $\dot{\varepsilon}^e_{v\,ch}$. The mechanical contribution is defined evaluated through the logarithmic compliance κ adopted in critical state soil mechanics. A similar parameter, the chemical elastic logarithmic compliance κ_π, is introduced to evaluate the chemical component. The whole elastic volumetric strain increment $\dot{\varepsilon}^e_v$ then reads:

401 $$\dot{\varepsilon}_v^e = \dot{\varepsilon}_{v\,mec}^e + \dot{\varepsilon}_{v\,ch}^e = \frac{\kappa}{v}\frac{\dot{p}'}{p'} + \frac{\kappa_\pi}{v}\frac{\dot{\pi}}{\pi+\pi_0} \quad (6)$$

402

403 where *v* is the specific volume, π_0 is a reference osmotic suction (e.g. 1 kPa) introduced to avoid
404 infinite values of v when π goes to zero and *p*' is the mean effective stress. The contribution of
405 osmotic suction to elastic shear strain is neglected, so that increment of elastic deviatoric strain
406 $\dot{\varepsilon}_s^e$ reads:

407 $$\dot{\varepsilon}_s^e = \frac{1}{3G}\dot{q} \quad (7)$$

408 where *G* is the (constant) shear modulus and *q* the deviator stress.

409

410 ## 4.3 Elastic-plastic behavior
411

412 The yield surface in the (p',q, π) space is defined on basis of a simple mathematical interpretation
413 of the chemo-mechanical response in the compression plane. The approach followed is inspired
414 by the proposal of Alonso et al. (1990) to account for the role of matric suction on the behaviour
415 of unsaturated non-expansive soils.
416 As shown in the previous sections, the position and the slope of the NCL depend on the fabric
417 imparted by the history of mechanical and chemical loads. Both the parameters that identify the
418 NCL in the compression plane (the specific volume *N* for a reference mean effective stress p'_r and
419 the elasto-plastic logarithmic compliance λ) may change with π. In the following, N_0 and λ_0 refer
420 to the soil saturated with distilled water, whereas $N(\pi)$ and $\lambda(\pi)$ refer to a generic saline solution
421 of osmotic suction π.

422 The preconsolidation pressure is expressed as p'_0 when the soil is saturated with distilled water
423 and it is expressed as p'_c (π) when the soil is saturated by the generic saline solution. The
424 mathematical link between p'_0 and p'_c can be obtained considering two different loading paths,
425 LPI and LPII in the stress plane (p', π) of Figure 8a and in the compression plane (v, ln p') of
426 Figure 8b.
427 Along loading path LPI a sample 'prepared' and saturated distilled water is loaded in virgin
428 conditions up to p'_0 (point A): during this stage it moves along the NCL corresponding to $\pi = 0$.
429 Osmotic suction is then increased to $\pi = \pi_C$ while the mean effective stress is kept constant: this
430 causes compressive elastic volumetric strains and the specific volume reduces (path AB in
431 Figure 8). From B, the mechanical stress is further increased while the osmotic suction is kept
432 constant. Elasto-plastic volume strains take place only when the specific volume lays on the NCL,
433 thus volume contraction will initially be elastic as the NCL (π_c) lays above the NCL ($\pi = 0$). Yielding
434 occurs when the elastic reloading line meets the NCL (π_c), i.e. at point C in Figure 8, where the
435 mean effective stress is p'_c and the specific volume is v_c. By further increasing the mechanical
436 stress, the behaviour will be elastoplastic and the sample will move along the NCL corresponding
437 to $\pi = \pi_C$.
438 Point C can also be reached through the loading path LPII, corresponding to mechanical loading
439 at constant osmotic suction $\pi = \pi_C$ of a specimen that has the same fabric of C. In the compression
440 plane, LPII marks the NCL(π_C) between $p' = p'_r$ and $p' = p'_c$.

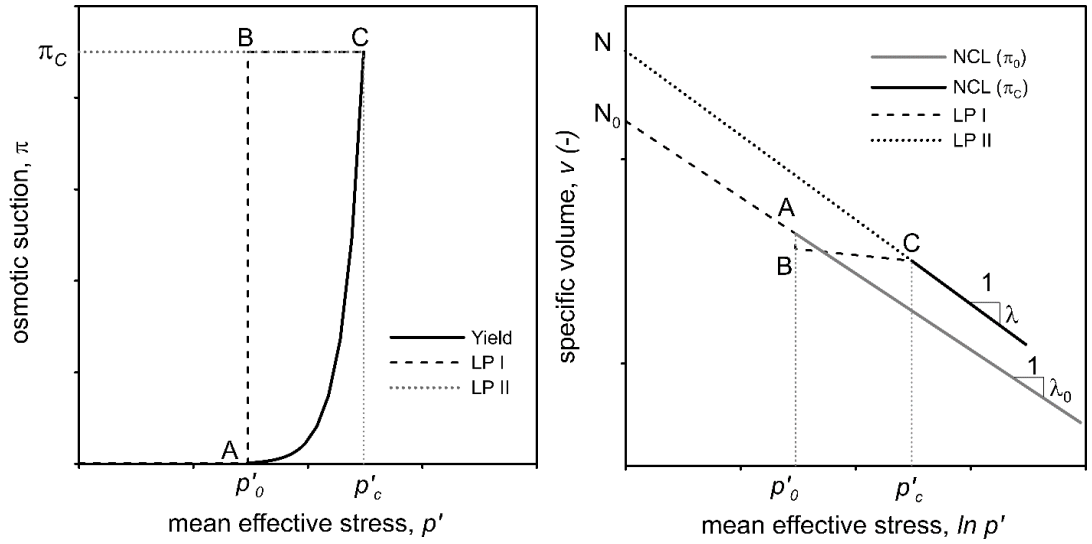

441 Fig. 8 a) Loading paths LPI and LPII and yield surface in the (p',π) plane; b) loading paths LPI and
442 LPII and Normal Compression Lines for the two different osmotic suctions
443

444 By evaluating v_c along LPI:

445 $$v_C = N_0 - \lambda_o ln\left(\frac{p'_0}{p'_r}\right) + \Delta v^{ch} - \kappa ln\left(\frac{p'_c}{p'_0}\right) \quad (8)$$

446 where Δv^{ch} is the elastic change in specific volume when the osmotic suction increases from 0

447 to π, evaluated with eq. (5):

448 $$\Delta v^{ch} = -\kappa_\pi ln\left(\frac{\pi + \pi_0}{\pi_0}\right) \quad (9)$$

449 By evaluating v_c along LPII:

450 $$v_C = N - \lambda\, ln\left(\frac{p'_c}{p'_r}\right) \quad (10)$$

451 By introducing (8) in (7) and equating with (9), it follows:

452 $$\frac{p'_c}{p'_0} = \left(\frac{p'_0}{p'_r}\right)^{\frac{\lambda_0-\lambda}{\lambda-\kappa}} \cdot e^{\frac{N-N_0}{\lambda-\kappa}} \cdot \left(\frac{\pi+\pi_0}{\pi_0}\right)^{\frac{\kappa_\pi}{(\lambda-\kappa)}} \quad (11)$$

Equation (10) provides the evolution of the yield mean stress p'_c with osmotic suction in isotropic conditions. Extension to more general axis-symmetric conditions is performed through the yield surface (f =0) of the Modified Cam Clay model:

$$f(p', q, p'_c) = \frac{q^2}{M^2} + p'(p' - p'_c) \quad (12)$$

where M is the slope of the Critical State Line in the (p', q). The isotropic hardening law of the Modified Cam Clay is used, with p'_0 as the internal variable:

$$\dot{\varepsilon}_v^{pl} = \frac{\lambda_0 - \kappa}{v_0} \frac{\dot{p}'_0}{p'_0} \quad (13)$$

where v_0 is the specific volume associated to p'_0. An associated flow rule is finally adopted.

Suitable expressions relating N and λ to osmotic suction are also introduced. In analogy with what observed for the liquid limits, whose evolution with concentration follows a logarithmic trend (Figure 1), the following expressions are proposed:

$$N(\pi) = N_0 + \beta \ln\left(\frac{\pi + \pi_0}{\pi_0}\right) \quad (14)$$

$$\lambda(\pi) = \lambda_0 + \eta \ln\left(\frac{\pi + \pi_0}{\pi_0}\right) \quad (15)$$

where β and η are model parameters.

4.4 Shape of the yield surface in the (p',π) space

The shape of the yield function of eq. (11) in the (p', π) is controlled by:

(i) the dependency of λ on osmotic suction $\left(\frac{p'_0}{p'_r}\right)^{\frac{\lambda_0 - \lambda}{\lambda - \kappa}}$,

(ii) the dependency N on osmotic suction $e^{\frac{N - N_0}{\lambda - \kappa}}$;

(iii) the value of osmotic suction itself $\cdot \left(\frac{\pi + \pi_0}{\pi_0}\right)^{\frac{\kappa_\pi}{(\lambda - \kappa)}}$

474 These three factors depend on the mineralogy and initial fabric of the clay, so they might have
475 different relevance for different clays or clay "preparations". For modelling purposes, two
476 simplified hypotheses might be of interest:

477 a) osmotic suction does not affect the position and the slope of the NCL. In this case eq. (10)
478 reduces to:

479 $$\frac{p'_c}{p'_0} = \left(\frac{\pi+\pi_0}{\pi_0}\right)^{\frac{\kappa_\pi}{(\lambda_0-\kappa)}} \quad (16)$$

480 which points out the effects of the elastic chemical strains on the preconsolidation pressure;
481 b) osmotic suction affects the position of the NCL but not its slope. According to Section 3,
482 this seems to be the case for many non-expansive clays. Eq. (10) reduces then to:

483 $$\frac{p'_c}{p'_0} = e^{\frac{N-N_0}{\lambda 0-\kappa}} \cdot \left(\frac{\pi+\pi_0}{\pi_0}\right)^{\frac{\kappa_\pi}{(\lambda 0-\kappa)}}, \quad (17)$$

484

485 The shape of the yield surface is consistent with the experimental evidences provided by
486 Torrance (1974) for Drammen clay and the ones collected in this study for Spigno Monferrato
487 clay, shown in Figure 9. Both cases refer to reconstituted samples prepared mixing the dry soil
488 powder with distilled water at a content higher than the liquid limit, and then loaded in the
489 oedometer according to the sequence LPI from Figure 8a.

490

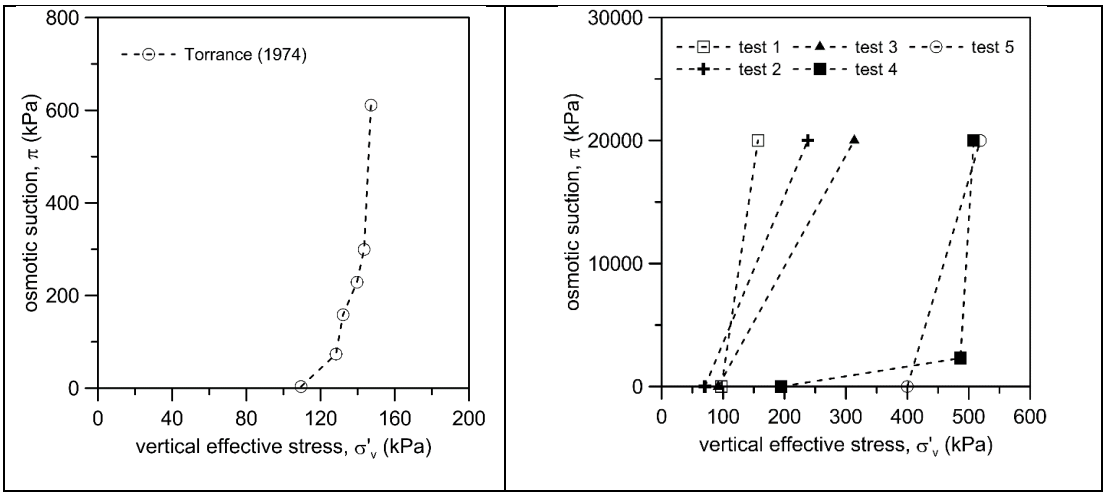

Fig- 9. Experimental data of dependency of the preconsolidation pressure on osmotic suction: a) Drammen clay (Torrance, 1974); b) Spigno Monferrato clay

5 Model validation for reconstituted, compacted and undisturbed soils

Since the mechanical behaviour of a given soil depends on the fabric imparted at its formation, the capabilities of the model were checked simulating oedometer tests performed on samples of reconstituted, compacted and undisturbed clays. To this extent, the model was implemented in a driver for the integration of the constitutive equations in rate form (see e.g. Cattaneo et al., 2011, 2014). The driver allows imposing histories of prescribed chemo-mechanical loading, which were assigned according with those adopted during the simulated experiments. In all the simulations, the reference osmotic suction was imposed as π_0 = 1 kPa.

5.1 Reconstituted Spigno Monferrato clay

The simulations of two oedometer tests run on reconstituted Spigno Monferrato clay were performed. The values of the parameter used in the simulation are reported in Table 2.

Table 2 Parameters and initial value of p'_0 used for the simulation of Spigno Monferrato clay

κ (-)	$\lambda_0 = \lambda$ (-)	κ_π (-)	ν (-)	M (-)	β (-)	p'_0 (kPa)
0.04	0.127	0.006	0.3	0.98	0.003	18

κ and λ were calibrated on the compression response of a sample prepared and mechanically loaded with distilled water as cell fluid, while κ_π was calibrated on the volumetric strains due to salinization of the first test described below. The dependence of N on pore fluid salinity was simulated with β = 0.003. The slope of the critical state line *M** was set equal to 0.98 and as a first approximation it was set independent from the chemical concentration of the pore fluid.

The two tests are characterized by different chemo-mechanical loading paths. The first one was provided in Figure 6 (experimental results in Figure 7). The predictions of the model, shown in Figure 10, are in good agreement with the experimental data. The model is capable of predicting volumetric shrinkage not only upon salinization (AA' and CC'), but also an irreversible void ratio reduction upon desalinization (BB'). In accordance with experimental data, the convex shape of the yield domain in the (p'-π) plane implies an elastic response due to mechanical loading after salinization and an elasto-plastic response due to mechanical loading after desalinization.

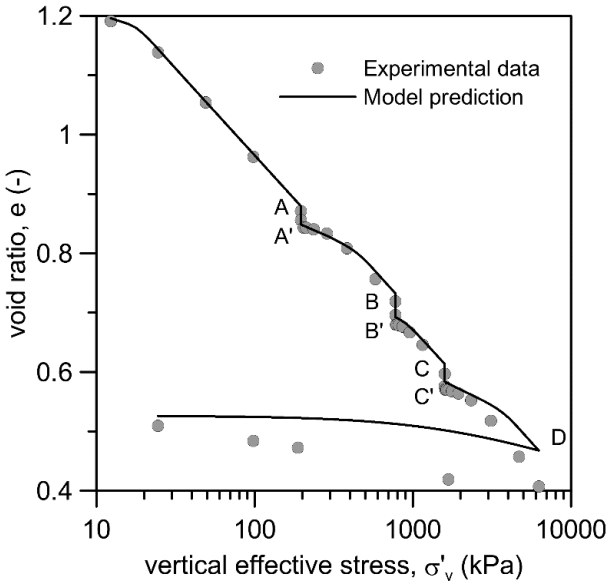

Fig 10 – Results of the simulation of the chemo-mechanical loading path performed on Spigno Monferrato clay of Figure 6.

The loading path in the salinity – vertical effective stress plane of the second oedometer test is provided in Figure 11a. The material was prepared with distilled water and then loaded up to a vertical stress $\sigma'_v = 98$ kPa (point A in Figure 11), then unloaded to $\sigma'_v = 74$ kPa (point B, OCR = 1.3). Following the same procedure described in Sec. 3.3, the concentration of the electrolyte in the cell fluid was increased to 4 M (NaCl) causing a decrease of volume up to point B'. Finally, the specimen was loaded up to a vertical stress $\sigma'_v = 6276$ kPa and finally unloaded to 24.5 kPa. The same parameters calibrated for the previous test were used in the simulation of this test, apart from the initial preconsolidation pressure here set equal to $p'_0 = 28$ kPa. The model correctly predicts volumetric shrinkage upon salinization and the consequent increase in preconsolidation pressure (Figure 11b), in very good agreement with the experimental data.

.

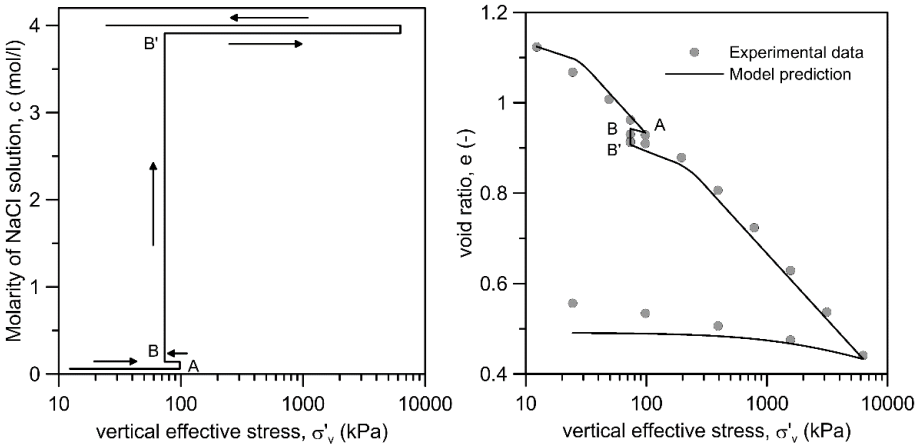

Fig 11 – (a) Loading path and (b) model predictions of the second chemo-mechanical test performed on Spigno Monferrato clay

5.2 Compacted illitic clay (Witteveen et al., 2013)

The capability of the model to reproduce the behaviour of compacted clays was checked simulating two oedometer tests performed by Witteveen et al. (2013) on a compacted illitic soil (liquid limit w_L = 54% and plasticity index PI = 24 %). Specimens have been prepared by mixing the powder of the soil with distilled water at a water content below the liquid limit (w = 39 %) and statically compacted in oedometer up to different vertical stresses (σ'_v = 30 kPa for test C1 and σ'_v = 77 kPa for test C2). According to the authors, water saturation was reached during static compaction. Under these vertical stresses the specimens have been exposed to a saturated NaCl saline solution: after suction equalization they have been loaded at constant suction to σ'_v=1000 kPa and finally unloaded. The stress paths in the (σ'_v - M) plane is shown in Figure 12. The parameters of the model were calibrated on the results of test C2 and then used to predicted the response for test C1: their values are provided in Table 3 together with the initial value of p'_0. The dependence of elasto-plastic compliance λ on pore fluid concentration was neglected, while

560 a small increase of *N* with osmotic suction was imposed (β = 0.0013). The comparisons between
561 model predictions and experimental data are shown in Figure 13. The model proves able to
562 reproduce with a very limited number of parameters the main features of the chemo-mechanical
563 response on non-active clays, also if prepared by compaction. Remarkably, the obtained shape
564 of the yield function in the (p'-π) plane allows a correct prediction of the elastic reloading stage
565 if the material is loaded after salinization.
566

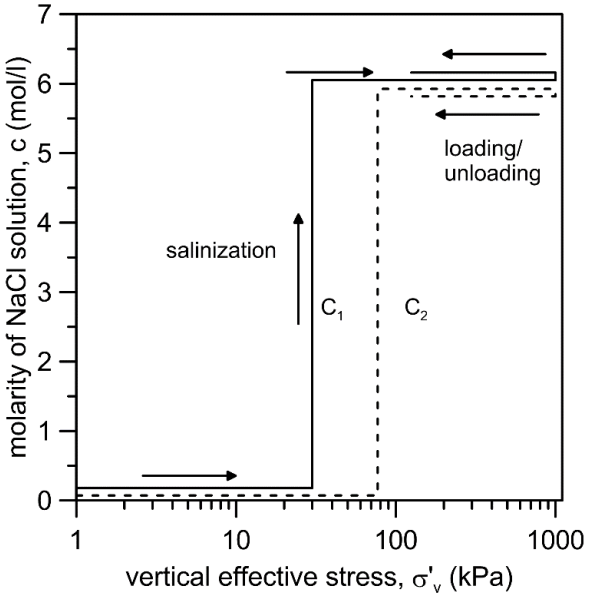

567

568 Fig 12. Chemo-mechanical loading path for compacted illitic soil (Witteveen et al, 2013)
569

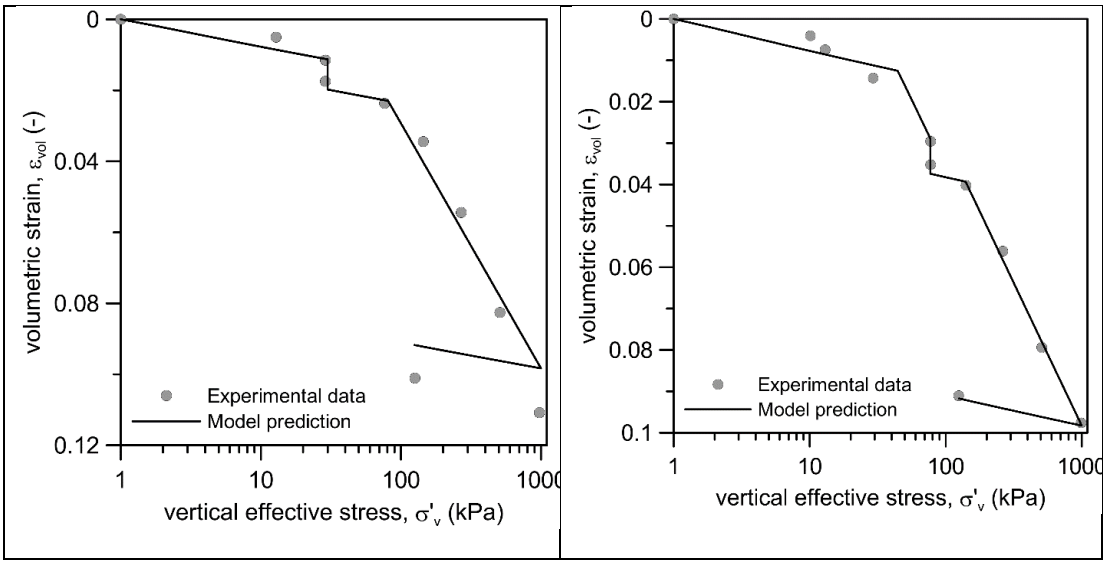

570 Fig- 13. Comparison between experimental data and model predictions for compacted illitic soil
571 in Witteveen et al, 2013. Specimens C1 (left) and C2 (right).
572
573 Table 3 Parameters and initial value of p'_0 used for the simulation of compacted illitic soil in
574 Witteveen et al. (2013)

κ (-)	λ_0 (-)	κ_π (-)	G (kPa)	M (-)	β (−)	p'_0 (kPa)
0.006	0.058	0.0016	67	0.98	1.3 e-3	43

575

576 ## 5.3 Intact and reconstituted quick clays
577
578 Torrance (1974) performed oedometer tests on undisturbed samples of intact Drammen clay, a
579 natural a low activity (w_L = 54 %, IP = 23 %, Activity = 0.46) Norwegian quick clay, whose pore
580 water has an initial (natural) salt concentration of 26 g/l (Torrance 1974). Undisturbed specimens
581 have been loaded up to 150 kPa, a value larger than the in situ preconsolidation pressure, and
582 then unloaded to 15 kPa, inducing an OCR equal to 10. Afterwards, the specimens have been
583 subjected to leaching (i.e. the exposure to a fluid with a smaller saline concentration than the
584 initial one) at constant vertical stress. The fluids used for the leaching process have different NaCl

585 concentrations, namely 0, 1, 2, 3, 4 and 8 g/l. After leaching, specimens have been loaded again.
586 The loading path is shown in Figure 14 for leaching with 0 g/l and 8 g/l of NaCl (c = 0 mol/l and
587 c = 0.14 mol/l respectively). Experimental results show desalinization-induced swelling and, upon
588 reloading, a reduction in the preconsolidation pressure with respect to the one induced by
589 previous loading. The entity of the reduction is larger the lower the salinity of the leaching fluid.
590 The results of the simulations referred to the specimens leached with 0 g/l and 8 g/l are reported
591 in Figure 15. The complete set of parameter values and the initial value of the p'_0 used in the
592 simulation are reported in Table 4. Again, the dependence of λ on pore fluid concentration was
593 neglected, without compromising the quality of the numerical predictions. The model correctly
594 reproduces not only the elastic and elasto-plastic response upon mechanical loading, but also the
595 magnitude of swelling upon leaching.
596
597

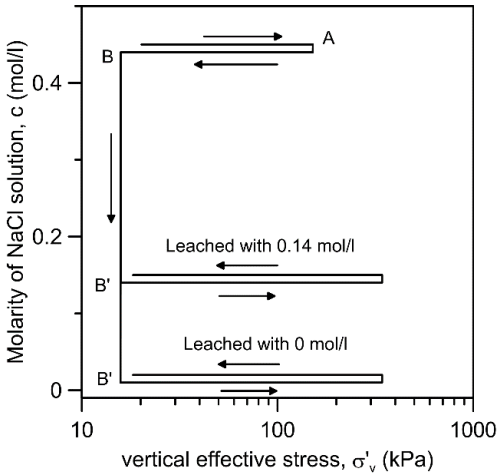

598
599 Fig- 14. Comparison between experimental data and model predictions for natural Drammen
600 clay (experimental data from Torrance, 1974)
601

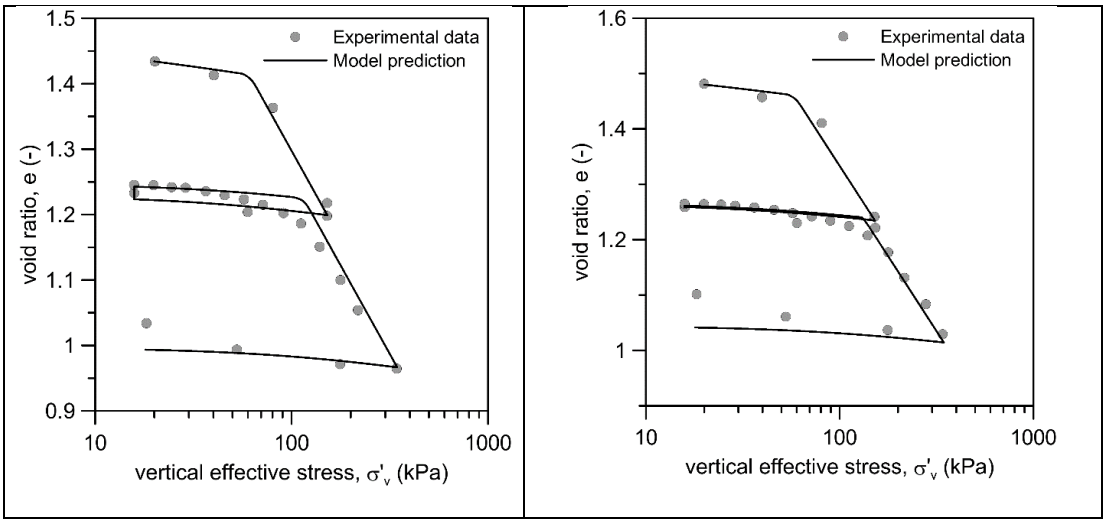

602 Fig- 15. Comparison between experimental data and model predictions for natural Drammen clay
603 (experimental data from Torrance, 1974). Leaching with distilled water (left) and with NaCl
604 solution with salt concentration 8 g/l (right)
605

606 Table 4 Parameters and initial value of p_0' used for the simulation of natural Drammen clay

κ (-)	λ_0 (-)	κ_π (-)	ν (-)	M (-)	β (−)	p_0' (kPa)
0.022	0.235	0.0031	0.3	0.98	4.8 e-3	39

607

608 A further validation of the model was performed against the results of oedometer tests on
609 Vaterland clay (w_L= 40 %, IP=16%, Activity=0.40), another Norwegian quick clay (Torrance, 1974).
610 Four specimens of Vaterland marine clay had been remoulded with a NaCl solution of
611 concentration 26 g/L (c = 0.44 mol/l) as saturating fluid, loaded in oedometer to a vertical
612 effective stress σ'_v = 18 kPa (point A in Fig. 16 a), and then unloaded to σ'_v = 6kPa (point B in
613 Fig. 16 a), inducing an OCR = 3. The specimens were then leached, i.e. exposed to distilled water
614 keeping the vertical stress constant (point B'): as consequence, the specimens experienced a
615 volume reduction. After leaching, three specimens had been exposed to potassium chloride at
616 different concentrations (namely K-low, K-medium and K-high, corresponding to 0.014 mol/l,

617 0.045 mol/l and 0.097 mol/l). One specimen, referred to as “leached specimen”, had only been
618 subjected to distilled water, without further changes in the pore fluid.
619 Afterwards, all the specimens had been reloaded to a vertical stress of 168 kPa. The loading paths
620 are shown in Figure 16 a, while the experimental data, as well as the model predictions, referring
621 to the leached specimen and to the specimen exposed to a medium concentration of potassium,
622 are shown in Figure 16 b.
623

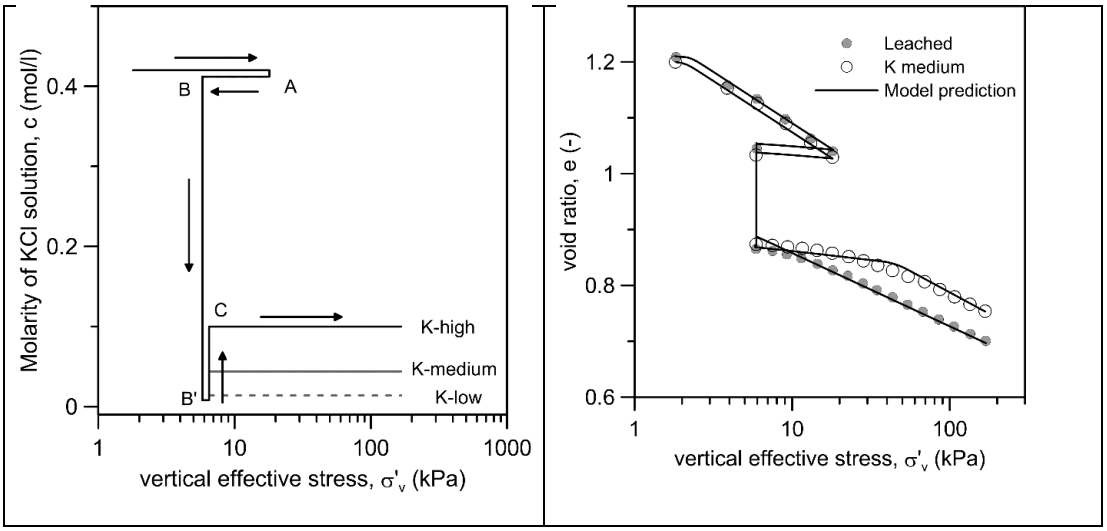

624 Fig- 16. Loading paths for Vaterland specimens leached with distilled water (BB’) and then exposed
625 to potassium chloride (B’C) (left); comparison between experimental data and model predictions
626 for the leached specimen and for the specimen exposed to a medium concentration of potassium
627 chloride (right) (experimental data from Torrance, 1974)
628

629 The experimental data confirm that the normal compression lines interpolating the virgin
630 compression branches tend to shift upwards in the compression plane at increasing electrolyte
631 concentrations. The model proved able to reproduce the volumetric collapse caused by leaching
632 of moderately overconsolidated specimens and the simulations are in good agreement with the
633 experimental results. The dependence of λ on π (see eq. 15) was considered and the parameters

634 adopted in the simulations are reported in Table 5. The proposed framework consistently
635 predicts that the preconsolidation pressure depends on the history of both mechanical and
636 chemical loadings: indeed, after volumetric collapse the leached specimen behaved as a normally
637 consolidated material, while the K-medium specimen behaved as an overconsolidated material.
638 Figure 17a presents model predictions for the three specimens exposed to potassium chloride.
639 Due to the shape of the yield function which expands with osmotic suction (Figure 17b), the yield
640 stresses increase at increasing salt concentration.

641

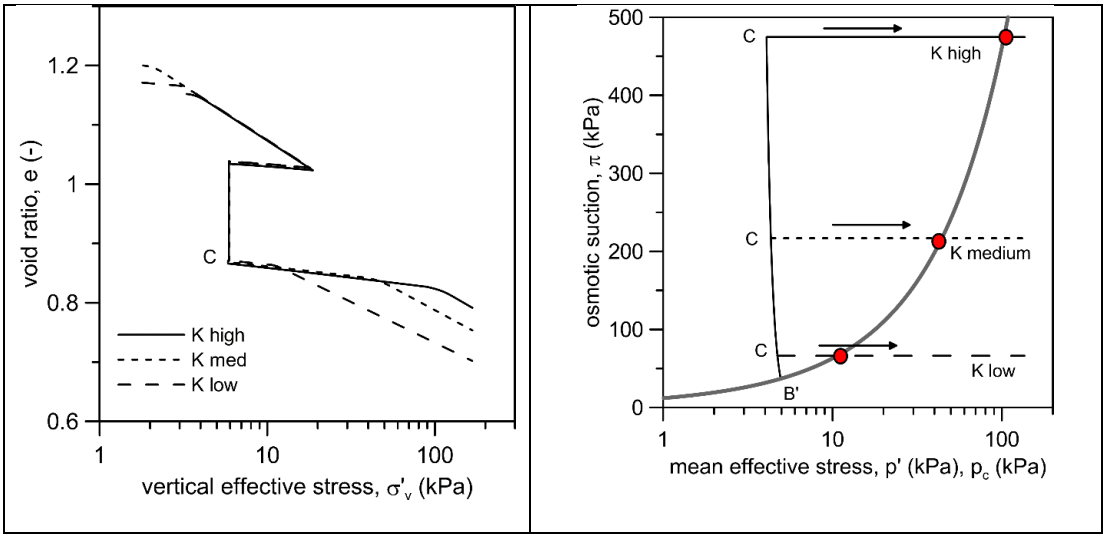

642 Fig- 17. (a) Simulation of tests with potassium addition; (b) shape of yield function in p'-π plane
643 during salinization (in bold black); stress paths referring to addition of potassium at different
644 concentrations and following reloading. Red points represent the intersection between the stress
645 path and the yield surface.
646
647 Table 5 Parameters and initial value of p_0' used for the simulation of Vaterland clay

κ (-)	λ_0 (-)	κ_π (-)	ν (-)	M (-)	β (–)	η (–)	p_0' (kPa)
0.015	0.04	0.003	0.3	0.98	0.045	0.002	1.0

648

6 Conclusions

The physico-chemical interaction between clay particles depends on the type of pore fluid and the mineralogy of the clay. The fabric of natural and reconstituted non-expansive illitic and smectitic clays in distilled water is mostly related to particle aggregation without flocculation, whereas it shows flocculation of particles or aggregates of particles in presence of dissolved salts. The flocculated fabric persists also when the stress is increased, whereas it is at least partially destroyed upon desalinization. The flocculated fabric is associated to larger pores with respect to the aggregated one, which helps explaining the experimental evidences that show the NCL of these soils moving to higher void ratios as the salt content increases. Changes in pore chemistry occurring under constant stress cause similar movements of the NCL, although to a limited extent. Even if the fabric of compacted soils is dominated by the effects of the mechanical load imparted in unsaturated conditions during compaction, the same effects seems to occur also for these soils. While changes in the thickness of the DDL alone would suggest an elastic type of behaviour, with volume contraction upon salinity increase and expansion upon salinity decrease, the experimental evidence shows that in normally consolidated non-expansive clays desalinitisation leads to inelastic compressive volume strains (collapse). These evidences at the phenomenological level resemble those observed for non-active unsaturated soils exposed to a decrease in matric suction. Their critical analysis lead to the proposal of an elasto-plastic model, which was formulated following the same procedure adopted by Alonso et al. (1990) for the Barcelona Basic Model (BBM). A yield function which expands with osmotic suction, governed by the elastic chemical compressibility and the variations in the position and slope of the NCL, follows naturally from this procedure. The role of such a yield function with respect to chemo-

671 mechanical plastic effects is analogous to the one played by the Loading Collapse (LC) in the BBM.
672 However, it is worth noting that the LC for unsaturated soils and the present yield function (eq.
673 10) account for different physical processes (LC for capillarity and the present one for salinity,
674 mediated through changes in fabric arrangements discussed previously).
675

676 Acknowledgments

677 The first author would like to acknowledge the contributions of Francesco Macario, MSc. and of
678 Mattia Minnite, Msc., which carried out the tests on Spigno Monferrato clay and on Illite. Thanks
679 are due also to Andrea Barillaro, geologist of BAAN Industrial Raw Materials, for providing the
680 pure Illite powder.
681

682 Notation

a_w	activity of water
c	molar concentration
e_L	void ratio at liquid limit with saline solution as saturating fluid
e_L^0	void ratio at liquid limit with distilled water as saturating fluid
i	number of species of the solute
M	slope of the Critical State Line in the *(p',q)* plane
N	intercept of the Normal Compression Line
N_0	Intercept of the Normal Compression Line with distilled water

p'	mean effective stress
p'_c	preconsolidation pressure
p'_r	reference mean stress
p'_0	preconsolidation pressure with distilled water
q	deviatoric stress
R	universal gas constant
T	absolute temperature
u	pore pressure
v	specific volume
v_w	molar volume of H_2O
β	model parameter describing the dependency of N on osmotic suction
δ_{ij}	Kronecker delta
$\dot{\varepsilon}_s^e$	increment of deviatoric strain
$\dot{\varepsilon}_{v\,ch}^e$	increment of elastic volume strain due to osmotic suction change
$\dot{\varepsilon}_{v\,mec}^e$	increment of elastic volume strain due to stress change
$\dot{\varepsilon}_v^e$	increment of elastic volume strain
η	model parameter describing the dependency of λ on osmotic suction
κ	elastic logarithmic mechanical compliance
κ_π	chemical elastic compliance
λ	elasto-plastic logarithmic mechanical compliance
λ_0	elasto-plastic logarithmic compliance at reference osmotic suction
π	osmotic suction

π_0	reference osmotic suction
σ_{ij}	component of total stress
σ'_{ij}	component of Terzaghi effective stress

683

684

References

Alonso EE, Gens A, and Josa A (1990) A constitutive model for partially saturated soils. Géotechnique **40(3)**: 405–430.

Barbour SL and Fredlund DG (1989) Mechanisms of osmotic flow and volume change in clay soils. Canadian Geotechnical Journal **26(4)**: 551–562.

Barbour SL and Yang N (1993) A review of the influence of clay-brine interactions on the geotechnical properties of Ca-montmorillonitic clayey soils from western Canada. Canadian Geotechnical Journal **30(6)**: 920–934.

Bjerrum L and Rosenqvist IT (1956) Some experiments with artificially sedimented clays. Géotechnique **6 (4)**: 124–136.

Cattaneo F Della Vecchia G and Jommi C (2011) A driver for the integration of coupled hydro-mechanical constitutive laws for unsaturated soils. In *Unsaturated soils: Proceedings of the Fifth International Conference on Unsaturated Soils. Barcelona* (Alonso EE and Gens A (eds)). Balkema, Rotterdam, The Netherlands, vol. 2, pp 1017-23.

Cattaneo F, Della Vecchia G and Jommi, C (2014) Evaluation of numerical stress-point algorithms on elastic–plastic models for unsaturated soils with hardening dependent on the degree of saturation. Computers and Geotechnics **55**: 404-415.

Collins KT and McGown A (1974). The form and function of microfabric features in a variety of natural soils. Géotechnique **24(2)**: 223–254.

Di Maio C (1996). Exposure of bentonite to salt solution: osmotic and mechanical effects. Géotechnique **46(4)**: 695-707.

706 Di Maio C, Santoli L and Schiavone P (2004) Volume change behaviour of clays: the influence of
707 mineral composition, pore fluid composition and stress state. Mechanics of Materials **36**: 435–
708 451.
709 Della Vecchia G, Jommi C and Romero E (2013). A fully coupled elastic–plastic hydromechanical
710 model for compacted soils accounting for clay activity. International Journal for Numerical and
711 Analytical Methods in Geomechanics, **37(5)**: 503-535.
712 Della Vecchia G and Musso G (2016). Some remarks on single-and double-porosity modeling of
713 coupled chemo-hydro-mechanical processes in clays. Soils and Foundations **56(5)**: 779-789.
714 Della Vecchia G Scelsi G and Musso G (2019) Modelling the role of pore water salinity on the
715 water retention behaviour of compacted active clays. Italian Geotechnical Journal (Rivista Italiana
716 di Geotecnica), **3**: 16-19
717 Gajo A and Loret B (2003). Finite element simulations of chemo-mechanical coupling in elastic–
718 plastic homoionic expansive clays. Computer Methods in Applied Mechanics and Engineering
719 **192(31-32)**: 3489-3530.
720 Guimarães L D N, Gens A, Sánchez M and Olivella, S (2013). A chemo-mechanical constitutive
721 model accounting for cation exchange in expansive clays. Géotechnique **63(3)**: 221-234.
722 Hueckel T (1997) Chemo-plasticity of clays subjected to stress and flow of a single contaminant.
723 International Journal for Numerical and Analytical Methods in Geomechanics **21(1)**: 43–72.
724 Jang, J and Santamarina, J C (2016). Fines classification based on sensitivity to pore-fluid
725 chemistry. Journal of Geotechnical and Geoenvironmental Engineering **ASCE 142(4)**: 06015018

726 Liu Z, Boukpeti N, Li X, Collin F, Radu J P, Hueckel T, and Charlier R (2005). Modelling chemo-
727 hydro-mechanical behaviour of unsaturated clays: a feasibility study. International Journal for
728 Numerical and Analytical Methods in Geomechanics, **29(9)**: 919-940.
729 Loret B, Hueckel T and Gajo A (2002). Chemo-mechanical coupling in saturated porous media:
730 elastic–plastic behaviour of homoionic expansive clays. International Journal of Solids and
731 Structures **39(10)**: 2773-2806.
732 Mitchell, J K and Soga, K (2005). *Fundamentals of soil behavior*. Wiley.
733 Musso G, Romero E, Gens A, and Castellanos E (2003). The role of structure in the chemically
734 induced deformations of Febex bentonite. Applied Clay Science, **23(1-4)**: 229–237.
735 Musso G, Chighini S and Romero E (2008). Mechanical sensitivity to hydrochemical processes of
736 Monastero Bormida clay. Water Resources Research, **44(5)**: W00C10.
737 Musso G, Romero E, and Della Vecchia G (2013). Double-structure effects on the chemo-hydro-
738 mechanical behaviour of a compacted active clay. Géotechnique, **63(3)**: 206-220.
739 Musso G, Cosentini RM, Dominijanni A, Guarena N and Manassero M (2017). Laboratory
740 characterization of the chemo-hydro-mechanical behaviour of chemically sensitive clays. Italian
741 Geotechnical Journal (Rivista Italiana Di Geotecnica), **3**:22–47.
742 Noorany, I (1984) Phase relations in marine soils. Journal of Geotechnical Engineering
743 **ASCE 110(4)**: 539 - 543
744 Ohtsubo M, Egashira K and Takayama M (1985). Properties of a low-swelling smectitic marine
745 clay of interest in soil engineering. Canadian Geotechnical Journal, **22(2)**: 241-245.
746 Palomino AM and Santamarina J C (2005). Fabric map for kaolinite: effects of pH and ionic
747 concentration on behaviour. Clays and Clay Minerals, **53(3)**: 211-223.

748 Rosenqvist, IT (1966). Norwegian research into the properties of quick clay—a review.
749 Engineering Geology, **1(6)**: 445-450.
750 Santamarina JC, Klein KA and Fam MA (2001). *Soils and waves: Particulate materials behavior,*
751 *characterization and process monitoring*. Wiley.
752 Santamarina JC, Klein KA, Palomino A and Guimaraes MS (2002). Micro-scale aspects of chemical-
753 mechanical coupling: Interparticle forces and fabric. In *Chemo-Mechanical coupling in clays: From*
754 *nano-structure to engineering applications*, *Maratea.* (Di Maio C, Hueckel T and Loret B (eds)).
755 Balkema, Rotterdam, The Netherlands, pp. 47–64.
756 Sposito, G (1984). *The surface chemistry of soils*. Oxford University PresS
757 Sridharan A and Rao GV (1973). Mechanisms controlling volume change of saturated clays and
758 the role of the effective stress concept. Géotechnique, **23(3)**: 359–382.
759 Sridharan A, Rao S and Murthy N (1986) Liquid limit of montmorillonite soils. Geotechnical
760 Testing Journal, **9(3)**: 156-159.
761 Sridharan A, Rao S and Murthy N (1988) Liquid limit of kaolinitic soils. Géotechnique, **38(2)**: 191-
762 198
763 Sridharan, A (1991). Engineering behaviour of fine grained soils. A fundamental approach. Indian
764 Geotechnical Journal, **21(2)**: 133-144.
765 Tamagnini C and Ciantia M (2016). Plasticity with generalized hardening: constitutive modeling
766 and computational aspects. Acta Geotechnica, **11(3)**: 595–623.
767 Torrance, JK (1974). A laboratory investigation of the effect of leaching on the compressibility
768 and shear strength of Norwegian marine clays. Géotechnique **24(2)**: 155-173.

769 Torrance JK and Ohtsubo M (1995) Ariake bay quick clays: a comparison with the general model.
770 Soils and Foundations, **35(1)**: 11-19.
771 Van Olphen, H (1977) *An introduction to clay colloid chemistry, for clay technologists, geologists,*
772 *and soil scientists.* 2nd edition, Wiley
773 Witteveen P, Ferrari A and Laloui L (2013) An experimental and constitutive investigation on the
774 chemo-mechanical behavior of a clay. Géotechnique, **63(3)**: 244-255.
775 Yan, R (2018). BBM-type constitutive model for coupled chemomechanical behavior of saturated
776 soils. ASCE International Journal of Geomechanics, **18(10)**: 06018023.